Institut für Kernphysik
Schloßgartenstraße 9
64289 Darmstadt

TECHNISCHE
UNIVERSITÄT
DARMSTADT

NJL model study of the QCD phase diagram using the Taylor series expansion technique

Untersuchung des QCD Phasendiagramms im NJL-Modell mittels einer Taylorentwicklung

Bachelor Thesis

David Scheffler

December 2007

Supervision:
Prof. Dr. Jochen Wambach
PD Dr. Michael Buballa

Zusammenfassung

In einem einfachen Nambu-Jona-Lasinio-Modell (NJL-Modell) wird das QCD Phasendiagramm untersucht. Zunächst wird eine übliche Mean-Field-Rechnung benutzt, anschließend wird das großkanonische thermodynamische Potential in sechster Ordnung nach μ/T ausgehend von $\mu/T = 0$ entwickelt. Die berechneten Entwicklungskoeffizienten werden mit dem Stefan-Boltzmann-Grenzfall für hohe Temperaturen und Daten von Gitterrechnungen aus [ADE$^+$05] verglichen. Insbesondere wird der Verlauf der Crossover-Linie über die reduzierte chirale Suszeptibilität berechnet und der kritische Endpunkt bestimmt.

Abstract

In a simple Nambu-Jona-Lasinio (NJL) model we investigate the QCD phase diagram, first by applying conventional mean field calculation, then using a Taylor series expansion of the grand thermodynamic potential to sixth order in powers of μ/T at $\mu/T = 0$. Resulting expansion coefficients are compared to the high temperature Stefan-Boltzmann limit and to results from lattice calculations [ADE$^+$05]. Special emphasis lies on the calculation of the crossover line via the reduced chiral susceptibility and determination of the critical endpoint.

Contents

1 Introduction

The physics of quarks and gluons is described by quantum chromodynamics (QCD) which is the theory of strong interaction. The strong interaction acts on a property called color charge like the electromagnetic interaction acts on electric charge. The fact that gluons which mediate the strong force also carry color charges makes the theory complicated.

Confinement as a central phenomenon of QCD causes, that physical particles have to be color neutral. That means that quarks are forced to form hadrons - either quark-antiquark pairs, mesons, or three quark states, baryons. At very large temperatures or densities quarks and gluons are deconfined and form a plasma, the quark-gluon plasma (QGP). It is believed that the QGP plays an important role in the development of the early universe. Quark-gluon plasmas are experimentally investigated at heavy ion colliders.

The QCD phase diagram illustrates in which phase quarks exist at a particular temperature and chemical potential. A simple phase diagram would show confined quarks in a region of low temperature and chemical potential, surrounded by a phase boundary and QGP outside. At the phase boundary confined and deconfined states are in equilibrium.

Calculations in lattice QCD, which is a non-pertubative approach to QCD, are frequently performed to analyze the structure of the QCD phase diagram. It is not possible to use standard techniques to calculate properties at finite quark chemical potential due to the so-called fermion sign problem [Phi07]. Several methods (compare [Phi07]) have been developed to circumvent that problem including a Taylor series expansion of the grand canonical potential in μ/T at $\mu/T = 0$. Groups like [ADE$^+$05] have used that method to estimate the location of a chiral critical point in the phase diagram.

Calculations at arbitrary temperature and quark chemical potential are readily possible in the Nambu-Jona-Lasinio model, which is an effective model for QCD. Thus we will apply the method of a Taylor series expansion to the NJL model and check for consistency against regular calculations for determining the crossover line and locating the chiral critical point.

2 The Nambu-Jona-Lasinio model

2.1 The NJL Lagrangian and its symmetries

The Nambu-Jona-Lasinio (NJL) model was originally developed by Nambu and Jona-Lasinio in 1961 to describe dynamical mass generation of hadrons in analogy to the BCS theory of superconductivity ([NJL61a] and [NJL61b]). At that time quarks were not yet discovered. Consequently, the NJL model does not include gluons and color charge. Nevertheless, the model was later successfully used as an effective theory for quarks. This is due to symmetries of the model which reflect symmetries of the strong interaction which we will discuss shortly. A comprehensive treatment of properties and symmetries of the NJL model can be found in [Rip97] or [Kle92].

The strong interaction is described by four-quark pointlike interactions instead of gluon exchange. A simple form of the NJL Lagrangian density for two quark flavors can be written as:

$$\mathcal{L} = \bar{\psi}(i\partial\!\!\!/ - \underline{m})\psi + G\left((\bar{\psi}\psi)^2 + (\bar{\psi}i\gamma_5\tau_a\psi)^2\right) \tag{2.1}$$

Here the first term is the free (Dirac) part for the quark fields ψ and $\bar{\psi} = \psi^\dagger\gamma_0$ with the bare mass matrix $\underline{m} = \mathrm{diag}(m_u, m_d)$. The latter terms denote scalar and pseudoscalar interactions with the coupling constant G. τ_a are the Pauli matrices in isospin space.

The most general symmetry is the invariance under a global phase transformation $U = \exp\{i\alpha\}$ which leads to baryon number conservation.

The bare masses of up and down quarks are (relative to hadron masses) approximately the same. Since in QCD (in contrast to QED) interactions are flavor-independent, this leads to an $N_f = 2$-fold degeneracy in flavor space. For simplicity, we assume the masses of up and down quark to be exactly the same: $m \equiv m_u = m_d$. Then the Lagrangian of the NJL model is invariant under isospin rotations $U = \exp\left\{-\frac{i}{2}\alpha_a\tau_a\right\}$, which form an $SU(2)_f$ group. Furthermore all interactions are independent of the color of the quarks. Therefore we have an $N_c = 3$-fold degeneracy in color space.

Chirality ("handedness") is a conserved property of elementary particles with zero mass. Chiral symmetry is explicitly broken by non-zero quark masses. This is also obvious in the NJL Langrangian due to the occurrence of $\bar{\psi}m\psi$. In the "chiral limit" ($m = 0$) the Lagrangian is invariant under a unitary transformation $U = \exp\left\{-\frac{i}{2}\gamma_5\ \alpha_a\tau_a\right\}$. We will see in section 2.5 that the ground state can violate chiral symmetry, even in the chiral limit. This behavior is known as spontaneous symmetry breaking and is one of the most important features of the NJL model.

There will be divergent integrals in the course of our calculations. Since the NJL model cannot be renormalized (e. g. [Kle92]), we will regularize it using a sharp 3-momentum cut-off for divergent integrals, which is commonly done. By doing that, one violates Lorentz covariance, but this is considered to be of minor importance [Bub05]. There are other regularization methods which obey Lorentz covariance like regularization in proper time and Pauli-Villars regularization, see e. g. [Kle92]. Further details of the regularization method is given at a later time.

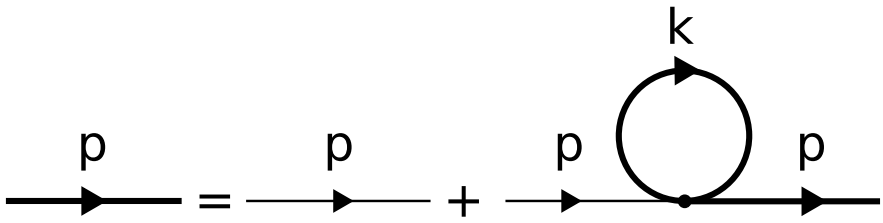

Figure 2.1: Diagrammatic self consistency equation involving dressed (bold line) and bare (thin line) quark propagators and a self-energy loop.

2.2 Effective quark mass at zero temperature and quark chemical potential

First of all we derive the effective quark mass in mean field approximation. We assign the single quark a current quark mass m. By coupling to itself via the scalar and pseudo-scalar channel (as included in the Lagrangian density), it gains an effective mass M, which is also known as the constituent quark mass. The necessary self-consistency equation is depicted in figure 2.1. For a quick guide to Feynman diagrams you might want to consider [Sch95].

The "bare" quark propagator with current quark mass m is given by

$$iS_0(p) = i\frac{\not{p} + m}{p^2 - m^2 + i\epsilon}, \tag{2.2}$$

and the propagator for a "dressed" quark with constituent (effective) quark mass M reads

$$iS(p) = i\frac{\not{p} + M}{p^2 - M^2 + i\epsilon}. \tag{2.3}$$

Having in mind figure 2.1 we can write down the self-consistency equation

$$iS(p) = iS_0(p) + iS_0(p)\ (-i\Sigma)\ iS(p), \tag{2.4}$$

where we defined the self-energy part in such a way that Σ is real. The self-energy can be expressed by $2iG$ times the sum of the outer products of each interaction channel. We also have to integrate over the free momentum k in the dressed quark propagator of the loop. The additional minus sign comes due to the fermion loop. Thus we have:

$$-i\Sigma = -i2G\left\{\mathbb{1}\int\frac{d^4k}{(2\pi)^4}\,\mathrm{Tr}\left[\mathbb{1}\ iS(k)\right] + i\gamma_5\tau_a\int\frac{d^4k}{(2\pi)^4}\,\mathrm{Tr}\left[i\gamma_5\tau_a\ iS(k)\right]\right\} \tag{2.5}$$

When evaluating the trace, all terms involving Pauli matrices or odd number of gamma matrices drop out. A factor of $4N_fN_c$ occurs due to the unit matrix in Dirac space and full degeneracy in flavor and color space. What remains for the self-energy is:

$$\Sigma = 2G\ 4N_fN_c\ M\ I(M) \tag{2.6}$$

with the integral

$$I(M) = i\int\frac{d^4k}{(2\pi)^4}\ \frac{1}{k^2 - M^2 + i\epsilon} \tag{2.7}$$

which can be evaluated using the residue theorem and further simplified using spherical coordinates:

$$I(M) = i \int \frac{d^3k}{(2\pi)^4} \int_{-\infty}^{\infty} dk_0 \, \frac{1}{k_0^2 - E_k^2 + i\epsilon} = \frac{1}{2} \int \frac{d^3k}{(2\pi)^3} \left(\frac{1}{E_k} \right) = \frac{1}{(2\pi)^2} \int_0^{\infty} dk \frac{k^2}{E_k}. \quad (2.8)$$

Here we already used k as the absolute value of the 3-momentum ($k \equiv |\vec{k}|$) and E_k as the single-particle energy $E_k \equiv E_k(k, M) = \sqrt{k^2 + M^2}$.

Now we come back to equation (2.4). Multiplying it from the left with the inverse propagator S_0^{-1} and from the right with S^{-1} brings us to a relation for the quark masses which is commonly called the gap equation:

$$M = m + \Sigma = m + 8\, N_f N_c G\; M\; I(M) \quad (2.9)$$

The integral in eq. (2.8) does not converge. When regularizing it using a 3-momentum cut-off Λ, one can solve it analytically:

$$I(M) = \frac{1}{(2\pi)^2} \int_0^{\Lambda} dk \; \frac{k^2}{E_k} = \frac{1}{(2\pi)^2} \; \frac{1}{2} \; \left(\Lambda \sqrt{\Lambda^2 + M^2} - M^2 \operatorname{arcsinh} \left[\frac{\Lambda}{M} \right] \right) \quad (2.10)$$

For a given set of parameters m, G, Λ it is now possible to solve the gap equation and to find an effective mass M.

2.3 Effective quark mass at finite temperature and quark chemical potential

When turning from quarks in vacuum to finite temperature T and chemical potential μ we need to apply the Matsubara formalism which results in the following important substitution on the integral occurring in the gap equation (2.9). A discussion on field theory at finite temperature goes beyond the scope of this thesis but can be found in [Kap89].

$$i \int \frac{d^4k}{(2\pi)^4} \; f(k) \longrightarrow -T \sum_n \int \frac{d^3k}{(2\pi)^3} \; f(i\omega_n + \mu, \vec{k}) \quad (2.11)$$

$$\text{with fermionic Matsubara frequencies} \quad \omega_n = (2n+1)\pi T$$

It can be solved by first using the residue theorem "backwards" to evaluate the Matsubara sum $(*)$. Next, the contour is transformed (see figure 2.2), and finally the residue theorem is used "forwards" using the new contour $(**)$, which now includes the two other poles.

$$\begin{aligned} I(T, \mu; M) &= -T \sum_n \int \frac{d^3k}{(2\pi)^3} \; \frac{1}{(i\omega_n + \mu)^2 - E_k^2} \\ &= \int \frac{d^3k}{(2\pi)^3} \; \frac{1}{2E_k} \left[-T \sum_n \left(\frac{1}{i\omega_n + \mu - E_k} - \frac{1}{i\omega_n + \mu + E_k} \right) \right] \\ &\overset{(*)}{=} \int \frac{d^3k}{(2\pi)^3} \; \frac{1}{2E_k} \frac{1}{2\pi i} \int_C dz \frac{1}{\exp(z/T) + 1} \left(\frac{1}{z + \mu - E_k} - \frac{1}{z + \mu + E_k} \right) \\ &\overset{(**)}{=} \int \frac{d^3k}{(2\pi)^3} \; \frac{1}{2E_k} - \int \frac{d^3k}{(2\pi)^3} \; \frac{1}{2E_k} \left[n_k + \bar{n}_k \right] \end{aligned} \quad (2.12)$$

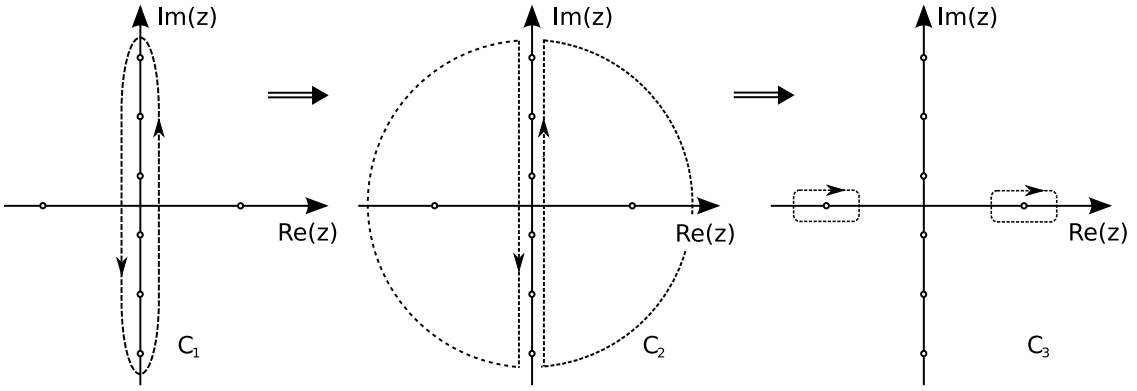

Figure 2.2: Deformation of the integration contour. Poles are indicated by small circles.

The result is expressed in terms of the quark and antiquark occupation numbers

$$n_k \equiv n(k,T,\mu;M) = \frac{1}{1+\exp\left(\frac{E_k-\mu}{T}\right)} \text{ and } \bar{n}_k \equiv \bar{n}(k,T,\mu;M) = \frac{1}{1+\exp\left(\frac{E_k+\mu}{T}\right)}. \tag{2.13}$$

The effective mass M is an auxiliary variable and thus will be separated from regular variables by a semicolon. Here we can recognize charge symmetry:

$$n(k,T,-\mu;M) = \bar{n}(k,T,\mu;M). \tag{2.14}$$

Plugging equation (2.12) into the gap equation (eq. (2.9)), we now can numerically search for a solution for the effective mass $M \equiv M(T,\mu)$, which of course depends on the temperature and quark chemical potential.

2.4 Thermodynamic potential

As there might be more than one solution to the gap equation, we need a criterion to decide which solution is the correct one. The common task in statistical physics is to minimize a thermodynamic potential. Since temperature and chemical potential are fixed, and the number of particles can vary, it is appropriate to use the grand canonical potential.

In a first step, we will linearize the Lagrangian density. For that purpose we need the expectation values of the interaction terms. The scalar interaction term gives rise to the so-called quark condensate or chiral condensate[1]:

$$\left\langle \bar{\psi}\psi \right\rangle_{NJL} = -i \int \frac{d^4k}{(2\pi)^4} \operatorname{Tr} S(k) \tag{2.15}$$

which in our case happens to be closely related to the constituent quark mass (compare eqs. (2.5) and (2.9)):

$$\left\langle \bar{\psi}\psi \right\rangle_{NJL} = -\frac{M-m}{2G} \tag{2.16}$$

[1]The definition of $\langle\bar{\psi}\psi\rangle$ is valid universally. The index NJL only emphasizes the sign convention.

The expectation value of the pseudo-scalar channel is zero since the trace over $i\gamma_5\tau_a S(k)$ vanishes.

Expanding $\bar{\psi}\psi = \langle\bar{\psi}\psi\rangle_{NJL} + \delta(\bar{\psi}\psi)$ using its expectation value $\langle\bar{\psi}\psi\rangle_{NJL}$ and dropping the quadratic term of the fluctuation, yields

$$(\bar{\psi}\psi)^2 \approx \langle\bar{\psi}\psi\rangle_{NJL}^2 + 2\langle\bar{\psi}\psi\rangle_{NJL}\,\delta(\bar{\psi}\psi) = 2\langle\bar{\psi}\psi\rangle_{NJL}\,\bar{\psi}\psi - \langle\bar{\psi}\psi\rangle_{NJL}^2 .$$

For the Lagrangian we obtain

$$\mathcal{L} \approx \bar{\psi}(i\partial\!\!\!/ - m)\psi + G\left(2\langle\bar{\psi}\psi\rangle_{NJL}\,\bar{\psi}\psi - \langle\bar{\psi}\psi\rangle_{NJL}^2\right) \tag{2.17}$$

$$= \bar{\psi}\left(i\partial\!\!\!/ - m + 2G\langle\bar{\psi}\psi\rangle_{NJL}\right)\psi - G\langle\bar{\psi}\psi\rangle_{NJL}^2 \tag{2.18}$$

We can express the Lagrangian in terms of an effective mass $M = m - 2G\langle\bar{\psi}\psi\rangle_{NJL}$:

$$\mathcal{L} = \bar{\psi}\left(i\partial\!\!\!/ - M\right)\psi - \frac{(M-m)^2}{4G} \tag{2.19}$$

This Lagrangian describes a free quark with mass M in an effective, constant potential. But we cannot drop the second term since we will have to vary M in order to find the stable mass.

The grand potential emerging from the Lagrangian consists of a free quark gas contribution which can be found in [Kap89] and the constant term from the Lagrangian:

$$\Omega_{NJL}(T,\mu;M) = \frac{(M-m)^2}{4G} - 2N_C N_F \frac{4\pi}{(2\pi)^3}\left\{\int_0^\Lambda dk\; k^2 E_k \right. \tag{2.20}$$

$$\left. + \int_0^\infty dk\; k^2\left[T\log\left(1+\exp\left[-\frac{E_k-\mu}{T}\right]\right) + T\log\left(1+\exp\left[-\frac{E_k+\mu}{T}\right]\right)\right]\right\}$$

An arbitrary constant can be added to the grand potential without changing the physics.

Here we applied the 3-momentum cut-off only to the first integral which would be divergent otherwise. The second integral does not diverge and contains the temperature dependence of the potential and may not be regularized for our purpose. It will become obvious in section 4.1 why this special regularization scheme is necessary.

One can easily confirm that the condition $\frac{\partial\Omega_{NJL}}{\partial M} = 0$ leads to the gap equation. The desired criterion for the correct mass is now obtained: a mass which satisfies the gap equation is an extreme value of the grand potential. But only the mass corresponding to the global minimum of the grand potential is the stable mass.

2.5 Numerical results

We are now ready to numerically calculate possible masses via the gap equation and determine the stable mass via the thermodynamic potential.

Parameters of the NJL model are the coupling constant G and the bare quark mass m. The regularization adds a third parameter, the 3-momentum cut-off Λ. Throughout this work

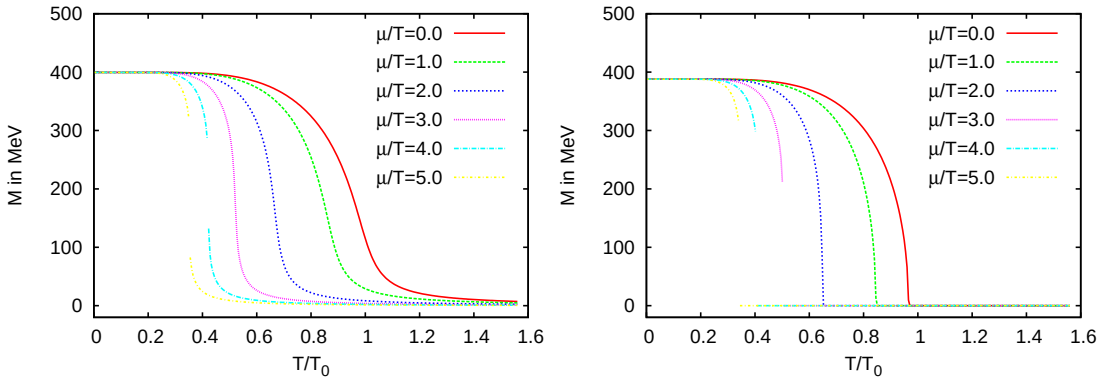

Figure 2.3: Effective mass for various μ/T as a function of T/T_0 at $m = 5.6$ MeV (left) and in the chiral limit (right).

the following parameter set will be used: $G = 2.44\ \Lambda^2$, $\Lambda = 587.9$ MeV and $m = 5.6$ MeV. These values are taken from [Bub05] where the parameters were determined in such a way that the model gives correct results for the pion mass m_π, the pion decay constant f_π and the quark condensate $\langle\bar{\psi}\psi\rangle$ in the vacuum ($T = \mu = 0$).

In figure 2.3 we see the effective mass for finite temperature and quark chemical potential. The temperature axis is given relative to a temperature T_0 which will be determined in section 3. In the present case we have $T_0 = 191.63$ MeV. In the left graph we have quarks with a small but finite bare mass. For small temperatures, the effective mass takes a value of about 400 MeV. With increasing temperature we see the effective mass drop to near zero MeV. The transition to small masses occurs earlier and more rapidly for higher values of μ/T. In the case of $\mu/T = 4.0$ and 5.0 there is a discontinuity at the transition. Between $\mu/T = 3.0$ and $\mu/T = 4.0$ there must exist a point where the gradient of M becomes infinite.

In the right graph the bare quark mass is set to zero (chiral limit). Even then the effective quark mass for small temperatures is about 400 MeV like in the massive case and drops to zero for higher temperatures. In comparison with the massive case the transition takes place earlier (at smaller temperatures). At the transition $M(T)$ is not continuously differentiable.

Here dynamic mass generation becomes visible. The major part of the effective mass arises due to the self-interaction, especially in the chiral limit. Since mass breaks chiral symmetry, chiral symmetry is broken by two effects: explicitly by the bare mass in the Lagrangian density, and spontaneously by the dynamically generated mass. For high temperatures and/or chemical potential the effective mass drops to a small value again, the symmetry is restored approximately. In the chiral limit, M goes to zero for high temperatures and/or chemical potential, and the chiral symmetry is fully restored.

Next we will investigate the behavior of the thermodynamic potential Ω_{NJL} as a function of the effective mass M. Figure 2.4 shows on the left side the thermodynamic potential for zero temperature and various values of the chemical potential. At $\mu = 0$ we have two minima at about ± 400 MeV and one maximum at about 0 MeV. The minimum for the positive mass is the global minimum of the potential and therefore the stable one. With rising chemical potential the central maximum lowers and a third minimum is formed. At

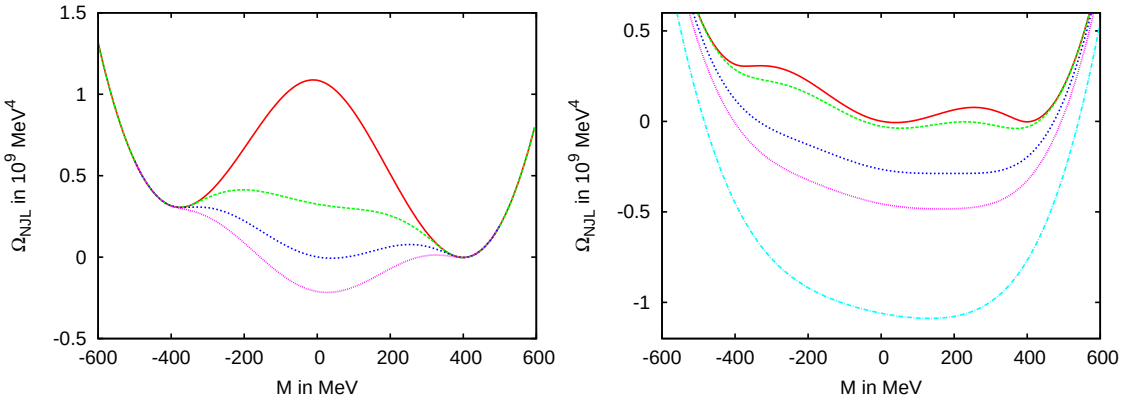

Figure 2.4: Thermodynamic potential as a function of the auxiliary variable M (constituent mass) at $T = 0$ (left) for $\mu = 0$ MeV, $\mu = 350$ MeV, $\mu = \mu_0 = 382.5$ MeV, $\mu = 400$ MeV (from top to bottom) and at several values on the phase boundary (right): $T = 0.0$ MeV, $\mu = 382.5$ MeV; $T = 40.0$ MeV, $\mu = 364.5$ MeV; $T = T_c = 82.2$ MeV, $\mu = \mu_c = 322.0$ MeV; $T = 100.0$ MeV, $\mu = 300.0$ MeV; $T = 139.8$ MeV, $\mu = 237.7$ MeV (from top to bottom). The potential has been shifted by an arbitrary constant.

a certain value $\mu = \mu_0$ the central minimum is at the same height as the right minimum. At that point, we have a first order phase transition, since the central minimum becomes the global minimum and the stable mass changes discontinuously.

On the right side of figure 2.4 we have the thermodynamic potential at several values along the phase boundary[2]. Starting at the top with $T = 0$ we have a first order phase transition as described before. With increasing temperature and at the same time decreasing chemical potential the central and right minimum approach each other. At a critical point with temperature T_c and chemical potential μ_c the two minima reach the same height in the diagram just when merging. This results in a vanishing curvature of Ω_{NJL} at that point. This is now a phase transition of second order since the stable mass changes continuously. For higher temperatures the mass varies smoothly from high to low values, and no actual phase transition takes place. This behavior is called a crossover transition.

2.6 Thermodynamic observables

After having studied the dependence of the thermodynamic potential Ω_{NJL} on the effective quark mass M, we will introduce thermodynamic observables which can immediately be calculated using derivatives of the grand potential.

Following the convention of [ADE+05], all observables can be given in a reduced way. The reduced thermodynamic potential is then given by

$$\Omega(T, \mu; M) = -\frac{1}{T^4}\, \Omega_{NJL}(T, \mu; M). \tag{2.21}$$

[2] will be calculated in the next section

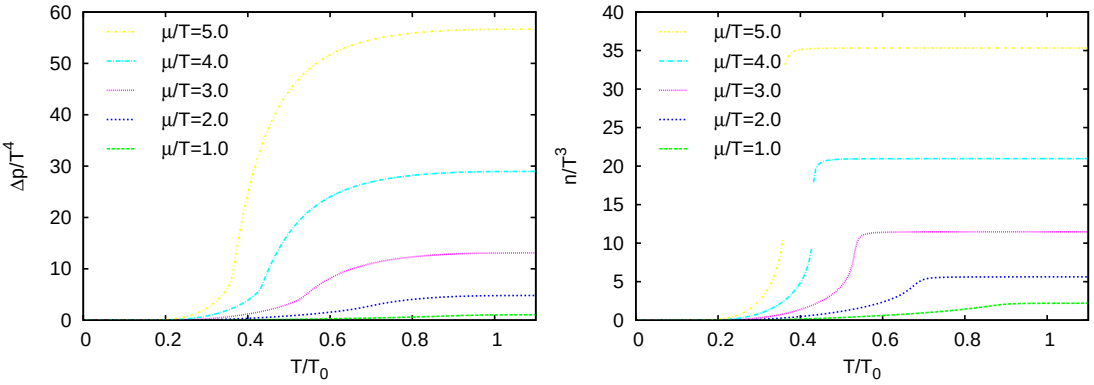

Figure 2.5: Reduced pressure (left) and reduced quark number density (right) as functions of T/T_0 for various μ/T.

We further define the reduced pressure such that it vanishes for zero temperature:

$$\frac{\Delta p(T,\mu)}{T^4} = \frac{p(T,\mu) - p(T,\mu=0)}{T^4} \tag{2.22}$$

where $p(T,\mu) = T^4\,\Omega(T,\mu) = -\Omega_{NJL}(T,\mu)$. The reduced quark number density reads

$$\frac{n(T,\mu)}{T^3} = T\frac{\partial\Omega}{\partial\mu} \tag{2.23}$$

In figure 2.5 we show the reduced pressure (left) and the reduced quark number density (right). The thermodynamic potential is continuous for all arguments. The quark number density becomes discontinuous at a first order phase transition and has infinite gradient at a second order phase transition.

The reduced chiral condensate appears as the first derivative of the thermodynamic potential with respect to the bare quark mass m.

$$\frac{\langle\bar\psi\psi\rangle(T,\mu)}{T^3} = T\frac{\partial\Omega}{\partial m} = -\frac{T}{T^4}\langle\bar\psi\psi\rangle_{NJL} = \frac{M-m}{2G\,T^3} \tag{2.24}$$

Several reduced susceptibilities can be defined via:

$$\frac{\chi_{ab}(T,\mu)}{T^2} = T^2\,\frac{\partial^2\Omega}{\partial a\,\partial b} \quad \text{with} \quad a,b \in T,\mu,m \tag{2.25}$$

So we obtain the reduced quark number susceptibility and the reduced chiral susceptibility:

$$\frac{\chi_{\mu\mu}}{T^2} = T^2\,\frac{\partial^2\Omega}{\partial\mu^2} \tag{2.26}$$

$$\frac{\chi_{mm}(T,\mu)}{T^2} = \frac{\partial^2\Omega}{\partial(\frac{m}{T})^2} = -T^{-2}\chi_{mm,NJL} = \frac{1}{2GT^2}\left(\frac{\partial M}{\partial m} - 1\right). \tag{2.27}$$

In figure 2.6 we show the reduced chiral susceptibility χ_{mm}/T^2 in the massive case (left) and in the chiral limit (right) for various values of μ/T. In the chiral limit we have a

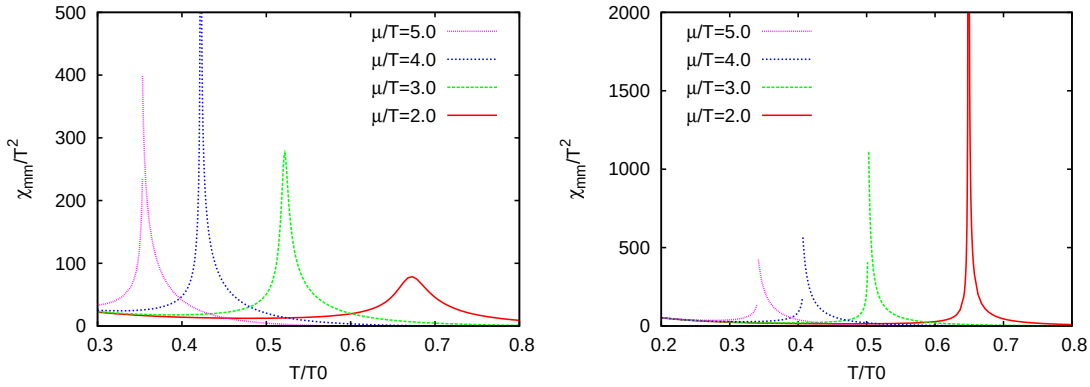

Figure 2.6: Reduced chiral susceptibility at $m = 5.6$ MeV and in the chiral limit ($m = 0$).

second order phase transition for $\mu/T = 2.0$, so the chiral susceptibility diverges[3]. In the massive case we only have a crossover transition. For the chiral susceptibility that means that it forms a finite maximum but does not diverge. For higher μ/T the peaks respectively maxima move to lower temperatures. At a first order phase transition the chiral susceptibility is discontinuous which occurs in the left figure for $\mu/T = 5.0$ and in the chiral limit (right) for $\mu/T = 3.0, 4.0$ and 5.0. For $m = 5.6$ MeV (left) $\mu/T = 4.0$ is close to the critical endpoint, where the transition is of second order. Therefore the peak takes a very high value.

2.7 High temperature limit

It is often appropriate to investigate certain limits of a model in order to check for consistency. In this section we will consider the high temperature limit.

We have seen that the effective mass M drops to about zero for high temperature and/or chemical potential. This corresponds to the case of a massless fermion gas with a degeneracy of $\nu = 2N_C N_F = 12$ (plus antiparticles) and is often called the Stefan-Boltzmann (SB) limit, since the calculation results in the typical T^4-behavior for the pressure. Please note that T^4 cancels out in the reduced pressure.

In the limit $M \to 0$ the first two terms of eq. (2.20) are independent of T and μ and therefore can be omitted. The remaining, explicitly temperature dependent part of the grand canonical potential can then be solved analytically:

$$\begin{aligned}\Omega_{SB} &= \lim_{M\to 0} -\nu \frac{4\pi T}{(2\pi)^3} \int_0^\infty dk\, k^2 \left[\log\left(1+\exp\left[-\frac{E_k-\mu}{T}\right]\right) + \log\left(1+\exp\left[-\frac{E_k+\mu}{T}\right]\right)\right] \\ &= -T^4 \cdot 2N_C N_F \left[\frac{7\pi^2}{360} + \frac{1}{12}\left(\frac{\mu}{T}\right)^2 + \frac{1}{24\pi^2}\left(\frac{\mu}{T}\right)^4\right] \end{aligned} \tag{2.28}$$

At a later point we will compare the Taylor series coefficients at high temperature with the coefficients found here in front of powers of μ/T.

[3]The value stays finite because of numerical issues (differential quotient). In comparison with the massive case (left), the peak height is two orders of magnitude higher which can be considered as “diverging”.

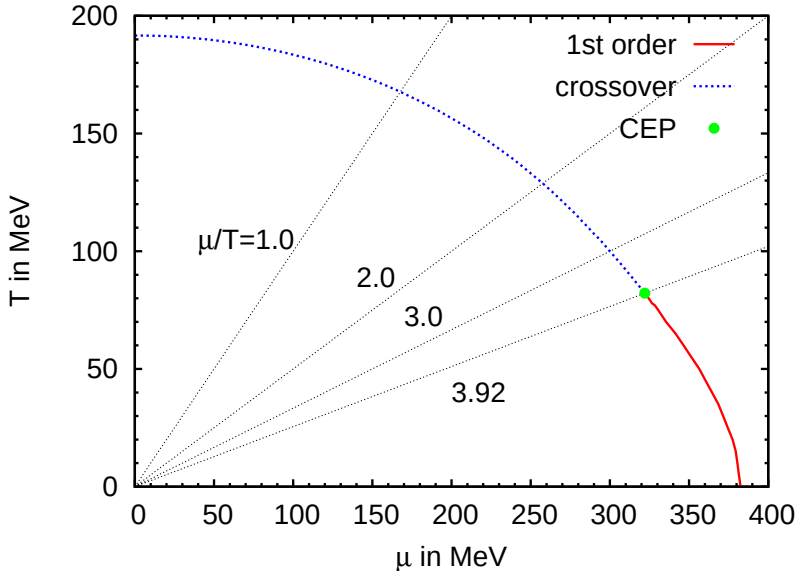

Figure 3.1: The phase diagram of the NJL model for parameters $G = 2.44\ \Lambda^2$, $\Lambda = 587.9$ MeV and $m = 5.6$ MeV. Lines of constant μ/T are indicated with dotted lines.

3 Phase diagram via exact calculation

Having motivated and introduced the Nambu-Jona-Lasinio model, we will now turn to the calculation and discussion of the phase diagram in the NJL model using exact[4] calculation.

We showed before, that the chiral susceptibility diverges at a second order phase transition and has a discontinuity at a first order phase transition. The quark number susceptibility shows the same behavior. For μ/T smaller than a certain value we have seen that there is no phase transition of first or second order. Instead, the effective quark mass drops rapidly and also other observables like the quark number density vary strongly in this region. This behavior was called a crossover transition. There is no unique definition of the crossover position in terms of physical observables. Possible choices are the position of maxima in the chiral susceptibility χ_{mm} or in the quark number susceptibility $\chi_{\mu\mu}$. The location of a maximum in the quark number susceptibility corresponds to the steepest rise of the quark number density which is an intuitive criterion.

To visualize the phase diagram we used the maximum of the reduced chiral susceptibility χ_{mm}/T^2 along lines of constant μ/T as the crossover criterion and the discontinuity of the mass as the criterion for a first order phase transition. We chose the reduced form particularly with regard to the convention introduced before.

The resulting phase diagram is shown in figure 3.1. For high chemical potential and low temperature (and therefore high μ/T), we find a first order phase transition. The phase

[4] To make the terminology clear: With "exact" we mean calculations using the full thermodynamic potential and derivated observables of the NJL model. Thereby we do not claim, that the NJL model, which is an effective quark model in mean-field approximation, is an exact description of QCD. Not an "exact" calculation in this sense is the Taylor series expansion introduced in the next section.

boundary ends in the so-called critical endpoint (CEP). For the studied parameter set the CEP is located at $T_c \approx 82.2$ MeV and $\mu_c \approx 322.0$ MeV which results in a critical ratio $(\mu/T)_c = \mu_c/T_c \approx 3.92$. At smaller μ/T we find a crossover transition.

The vacuum transition temperature $T_0 = 193.6$ MeV is determined by the temperature where the reduced chiral susceptibility χ_{mm}/T^2 for $\mu = 0$ has its maximal value. T_0 is used as a reference scale for all occurring temperatures.

4 Phase diagram via a Taylor series expansion

4.1 Taylor series expansion of the thermodynamic potential

As a second step, we will expand the thermodynamic potential to sixth order in μ/T and use the resulting Taylor series coefficients to determine features of the phase diagram.

The thermodynamic potential at arbitrary chemical potential can be expressed by the values of the derivatives of the thermodynamic potential with respect to the chemical potential evaluated at $\mu = 0$. This is known as a Taylor series expansion of the thermodynamic potential at zero chemical potential

$$\Omega_{NJL}(T,\mu) = \sum_n d_n(T)\ \mu^n \tag{4.1}$$

with coefficients

$$d_n(T) = \frac{1}{n!}\ \frac{d^n \Omega_{NJL}}{d\mu^n}\bigg|_{\mu=0}. \tag{4.2}$$

As the potential is symmetric in μ due to charge symmetry (compare eq. (2.14)) only even coefficients are nonzero:

$$d_{2m}(T) = \frac{1}{m!}\ \frac{d^m \Omega_{NJL}}{d(\mu^2)^m}\bigg|_{\mu=0}. \tag{4.3}$$

The reduced potential can be expanded in the dimensionless ratio μ/T at vanishing chemical potential:

$$\Omega(T,\mu) = \sum_n c_n(T) \left(\frac{\mu}{T}\right)^n \tag{4.4}$$

which is connected to Ω_{NJL} by

$$\Omega = -\Omega_{NJL} \cdot T^{-4} \quad \text{resp.} \quad \Omega_{NJL} = -\Omega \cdot T^4. \tag{4.5}$$

Ω is known as the reduced pressure p/T^4 in the NJL model. This immediately gives the conversion between the coefficients $c_n(T)$ and $d_n(T)$

$$c_n(T) = -d_n(T) \cdot T^{n-4} \quad \text{resp.} \quad d_n(T) = -c_n(T) \cdot T^{4-n}. \tag{4.6}$$

We calculated the expansion coefficients for $n = 2, 4$ and 6 for the given parameter set as functions of T. Derivatives of the thermodynamic potential give integrals which need to be evaluated numerically. The derivation of the necessary integrals and the integrals themselves are listed in the appendix.

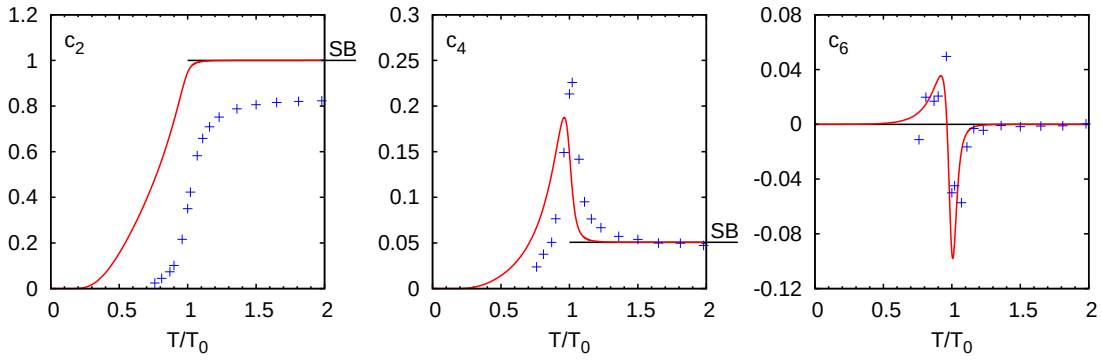

Figure 4.1: Taylor expansion coefficients c_n for $n = 2, 4, 6$ as functions of T/T_0 (lines). Also shown are results from [ADE+05] (points) and the Stefan-Boltzmann limits for high temperatures.

In figure 4.1 we show the Taylor expansion coefficients c_n for $n = 2, 4, 6$ as functions of T/T_0. Additionally we included results from [ADE+05] to compare both results.

All three coefficients vary smoothly and begin at zero for zero temperature. From c_2 to c_4 and from c_4 to c_6 the scale drops by about one order of magnitude. c_2 approaches the high temperature limit (SB) at $T > T_0$ from below. c_4 has a positive peak at a temperature slightly smaller than T_0 and then approaches the SB limit at $T > 1.1\ T_0$ from above. The coefficient c_6 also starts at zero, has a positive peak at about $0.9\ T_0$, and a negative peak at T_0. In between there is a zero-crossing. c_6 approaches zero from below for $T > 1.1\ T_0$.

The high temperature behavior of the coefficients c_2 and c_4 complies perfectly with the Stefan-Boltzmann limits calculated in section 2.7: $c_2(T > T_0) \to \frac{2N_C N_F}{12} = 1$ and $c_4(T > T_0) \to \frac{2N_C N_F}{24\pi^2} \approx 0.05$. This only happens due to the special regularization, which was used. If one would cut off the integral of the temperature influence, the coefficients c_2 and c_4 would overall be smaller and would drop to zero for high temperatures.

A rigorous comparison with the results from [ADE+05] is not reasonable. The underlying models are entirely different and also the used parameters are not comparable. For example in lattice calculations the mass depends linearly on the temperature. Still we will compare the features of the expansion coefficients, more qualitatively than quantitatively. We can recognize that the general behavior is similar. The lattice results for c_2 are overall smaller and do not reach the SB limit. Also the ascent occurs at a higher temperature. For c_4 the peak is located at a slightly higher temperature, and the SB limit is approached quite well this time. We should note that the statistical errors of the lattice results in the case of c_6 are 20% to 80% of the absolute values. The zero crossing is approximately located at T_0.

4.2 Thermodynamic observables

We will now revisit the reduced pressure and the reduced quark number density which have been introduced in section 2.6. We can easily express those observables in terms of

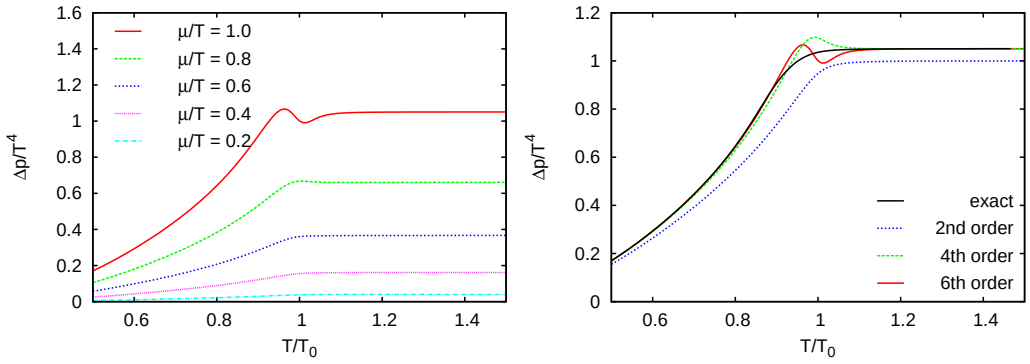

Figure 4.2: Reduced pressure at various μ/T to 6th order (left) and at $\mu/T = 1.0$ to 2nd, 4th and 6th order in comparison with exact calculations (right).

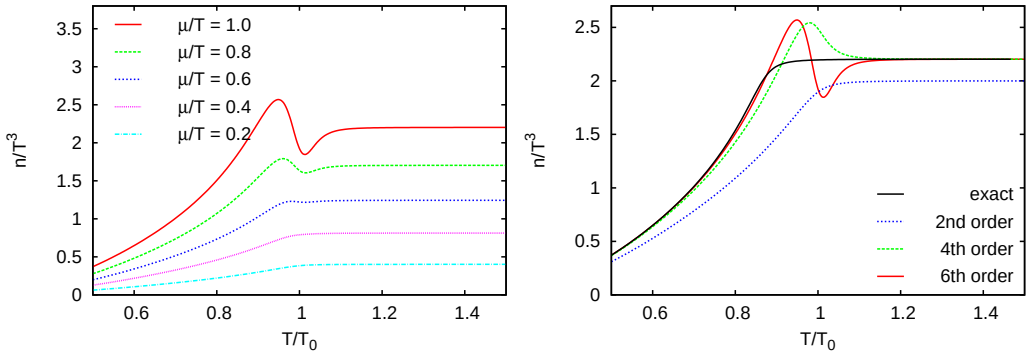

Figure 4.3: Reduced quark number density at various μ/T to 6th order (left) and at $\mu/T = 1.0$ to 2nd, 4th and 6th order in comparison with exact calculations (right).

the expansion coefficients:

$$\frac{\Delta p(T,\mu)}{T^4} = c_2(T)\left(\frac{\mu}{T}\right)^2 + c_4(T)\left(\frac{\mu}{T}\right)^4 + c_6(T)\left(\frac{\mu}{T}\right)^6 \tag{4.7}$$

$$\frac{n(T,\mu)}{T^3} = 2\,c_2(T)\left(\frac{\mu}{T}\right) + 4\,c_4(T)\left(\frac{\mu}{T}\right)^3 + 6\,c_6(T)\left(\frac{\mu}{T}\right)^5 \tag{4.8}$$

The reduced pressure $\Delta p/T^4$ is shown in figure 4.2. On the left side we show the reduced pressure for various μ/T to sixth order. We observe that the amplitude of the reduced pressure rises with increasing μ/T. At a temperature shortly above T_0 the reduced pressure saturates, which means, that the pressure p changes proportional to T^4. For $\mu/T = 1$ we recognize a dip at $T = T_0$. This can be seen more clearly on the right side where we compare the expansion to second, fourth and sixth order to the exact values exemplarily for $\mu/T = 1.0$. The dip at $T = T_0$ arises not until the inclusion of the sixth order term. To fourth order we have an overshoot. It would be interesting to see whether higher orders would compensate the dip. Apart from that region, higher order terms make the curve approach the exact line.

Very similar behavior can be found in the investigation of the reduced number quark density n/T^3. In figure 4.3 we can see that the dip at $T = T_0$ already forms at $\mu/T = 0.8$.

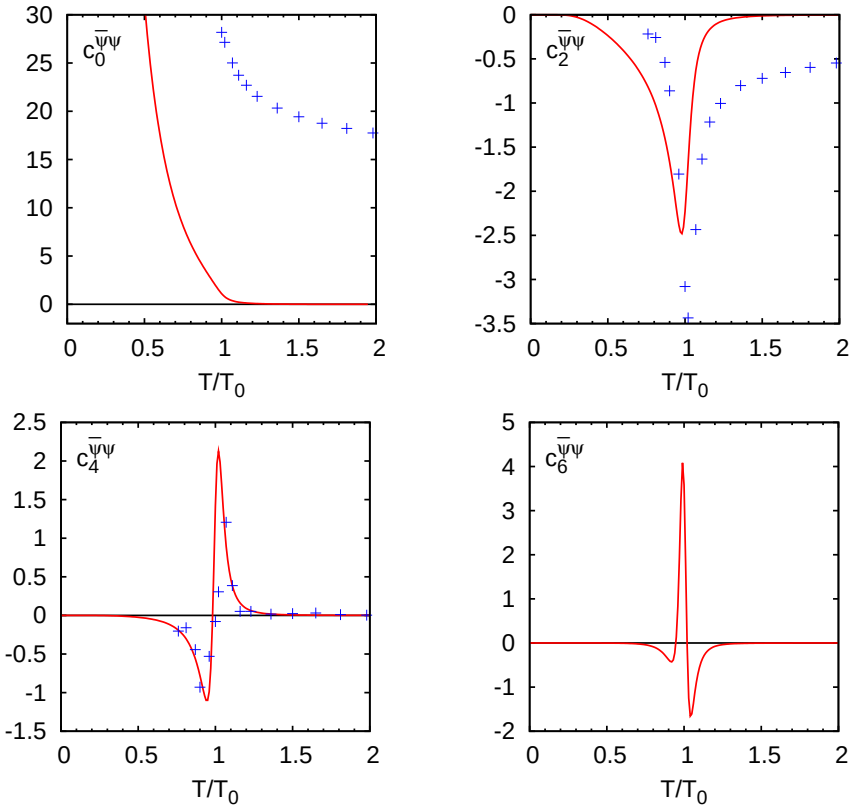

Figure 4.4: Taylor expansion coefficients $c_n^{\bar\psi\psi}$ for $n = 0, 2, 4, 6$ as functions of T/T_0 (lines). Also shown are results from [ADE+05] (points).

The next derivative with respect to the quark chemical potential yields the quark number susceptibility:

$$\frac{\chi_{\mu\mu}(T,\mu)}{T^2} = 2\, c_2(T) + 12\, c_4(T) \left(\frac{\mu}{T}\right)^2 + 30\, c_6(T) \left(\frac{\mu}{T}\right)^4 \tag{4.9}$$

Turning to derivatives of the grand potential with respect to the bare quark mass m, the first result is the chiral condensate $\langle\bar\psi\psi\rangle$.

$$\frac{\langle\bar\psi\psi\rangle}{T^3} = c_0^{\bar\psi\psi}(T) + c_2^{\bar\psi\psi}(T) \left(\frac{\mu}{T}\right)^2 + c_4^{\bar\psi\psi}(T) \left(\frac{\mu}{T}\right)^4 + c_6^{\bar\psi\psi}(T) \left(\frac{\mu}{T}\right)^6 \tag{4.10}$$

where the coefficients $c_n^{\bar\psi\psi}$ for $n = 2, 4$ and 6 can be calculated using a central difference quotient:

$$c_n^{\bar\psi\psi}(T) = \frac{\partial c_n(T)}{\partial m} \approx T\, \frac{c_n(T; m+\Delta) - c_n(T; m-\Delta)}{\Delta} \tag{4.11}$$

The zeroth order coefficient can be computed using the effective mass at zero chemical potential.

$$c_0^{\bar\psi\psi}(T) = \left.\frac{\langle\bar\psi\psi\rangle}{T^3}\right|_{\mu=0} = \frac{M(T,\mu=0) - m}{2G\, T^3} \tag{4.12}$$

The expansion coefficients $c_n^{\bar\psi\psi}$ of the reduced chiral condensate are plotted in figure 4.4.

We added the coefficients $c_0^{\bar{\psi}\psi}$, $c_2^{\bar{\psi}\psi}$ and $c_4^{\bar{\psi}\psi}$ presented in [ADE+05] for comparison. The leading order coefficient diverges for $T \to 0$ which is obvious from eq. (4.12) since the constituent mass is finite for $T \to 0$. It drops rapidly to a small negative value. Since the integrals in the gap equation have different upper limits the stable mass solution M does not approach m in the limit of high temperatures. The chiral condensate is proportional to $M - m$ and thus becomes negative for high temperatures. This is a disadvantage of the regularization and becomes visible at this point. The lattice data points lie much higher and are hardly comparable.

In the further coefficients we find $n/2$ peaks of alternating sign close to T_0. It is remarkable that the peaks become more narrow with increasing n. The location of the peak in the lattice data for $c_2^{\bar{\psi}\psi}$ is about the same as for our data. However the lattice data do not approach zero as fast as our results do. The lattice data for $c_4^{\bar{\psi}\psi}$ fit surprisingly well to our results.

4.3 Calculating the crossover line

Our next goal is to calculate the crossover line using the Taylor expansion coefficients. We have seen in section 2.6 that the chiral susceptibility diverges at a second order phase transition. So one possible definition of the crossover line is to take the point where the chiral susceptibility reaches its maximum, which was already used in the previous section.

The chiral susceptibility can be expressed using second derivatives of the Taylor coefficients with respect to the bare quark mass.

$$\frac{\chi_{mm}(T,\mu)}{T^2} = T^2 \, \frac{\partial^2 \Omega}{\partial m^2} = \sum_n T^2 \frac{\partial^2 c_n(T)}{\partial m^2} \left(\frac{\mu}{T}\right)^n = \sum_n c_n^\chi(T) \left(\frac{\mu}{T}\right)^n \tag{4.13}$$

$$= c_0^\chi(T) + c_2^\chi(T) \left(\frac{\mu}{T}\right)^2 + c_4^\chi(T) \left(\frac{\mu}{T}\right)^4 + c_6^\chi(T) \left(\frac{\mu}{T}\right)^6 \tag{4.14}$$

The coefficients $c_n^\chi(T)$ are calculated using a central second order difference quotient using the basic expansion coefficients $c_n(T)$, which need to be calculated at three slightly different bare quark masses:

$$c_n^\chi(T) = T^2 \, \frac{\partial^2 c_n(T)}{\partial m^2} \approx T^2 \, \frac{c_n(T; m+\Delta) - 2c_n(T;m) + c_n(T; m-\Delta)}{\Delta^2}, \quad n = 2, 4, 6 \tag{4.15}$$

The zeroth order coefficient c_0^χ needs to be calculated separately:

$$c_0^\chi(T) = T \, \frac{\partial c_0^{\bar{\psi}\psi}(T)}{\partial m} \approx T \, \frac{c_0^{\bar{\psi}\psi}(T; m+\Delta) - c_0^{\bar{\psi}\psi}(T; m-\Delta)}{\Delta} \tag{4.16}$$

with $c_0^{\bar{\psi}\psi}$ given in equation (4.12).

Resulting coefficients $c_n^\chi(T)$ are shown in figure 4.5. Again we can see that peaks occur in the vicinity of T_0, this time we have $n/2 + 1$ peaks with alternating sign. The amplitude of the peaks is growing with n and the peaks become more narrow. A surprising fact is that

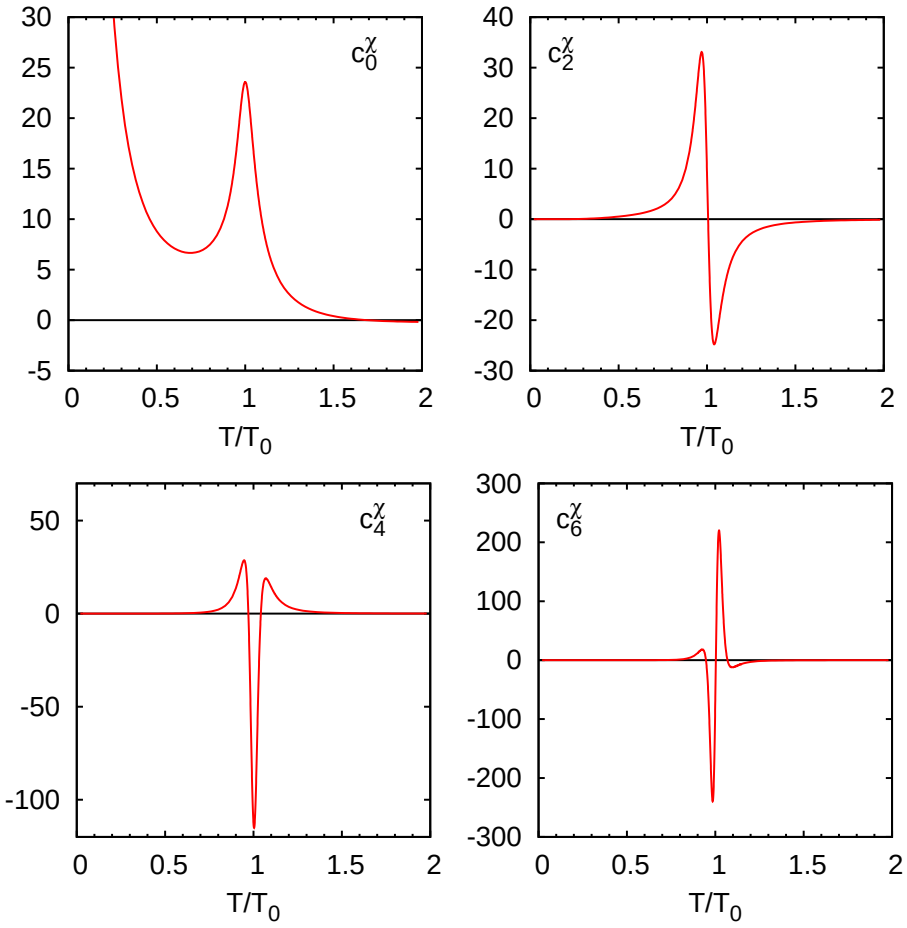

Figure 4.5: Taylor expansion coefficients c_n^χ for $n = 0, 2, 4, 6$ as functions of T/T_0.

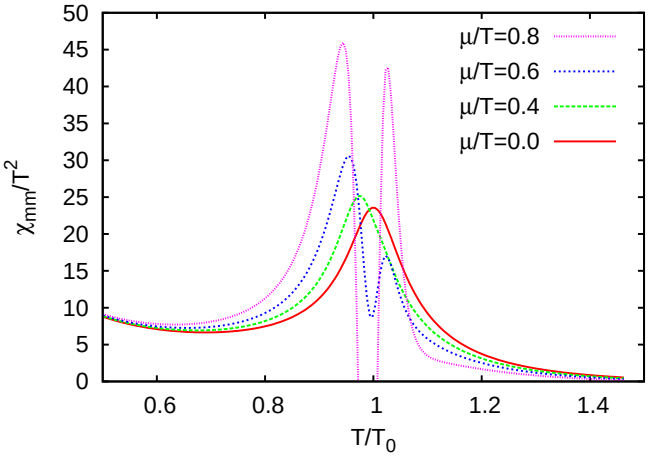

Figure 4.6: Reduced chiral susceptibility at various μ/T to 6th order.

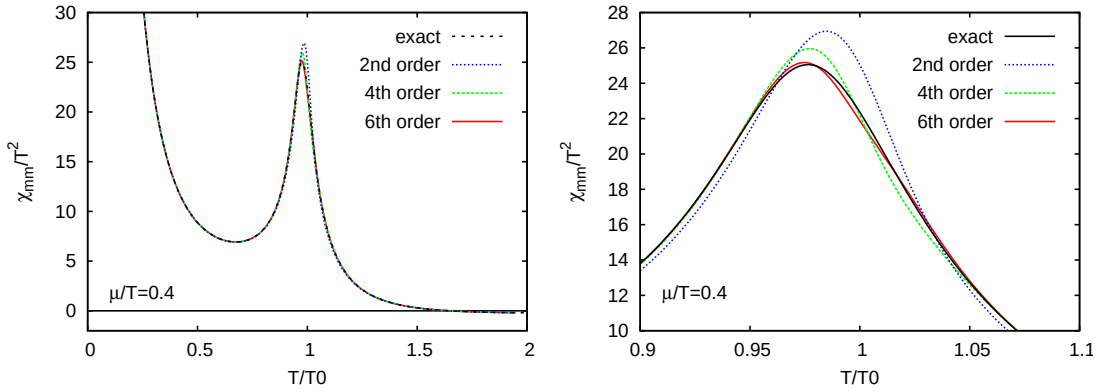

Figure 4.7: Reduced chiral susceptibility at $\mu/T = 0.4$ to 2nd, 4th and 6th order in comparison with exact calculations as an overview (left) and an enlarged section (right).

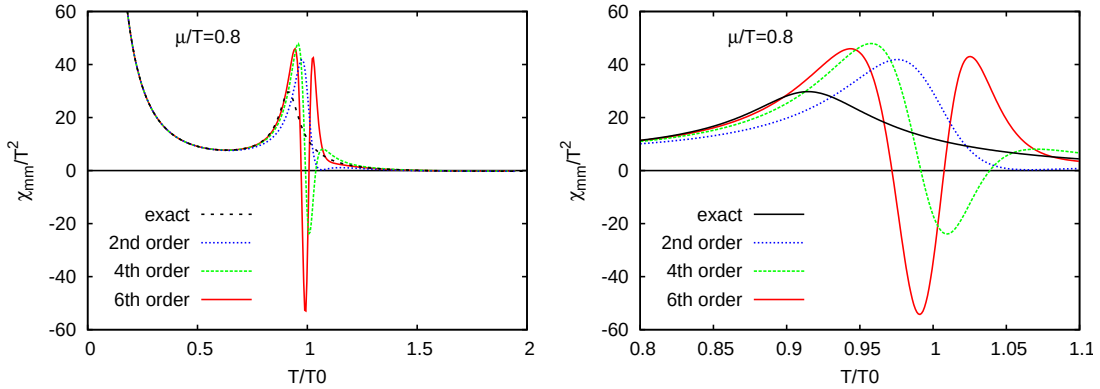

Figure 4.8: Reduced chiral susceptibility at $\mu/T = 0.8$ to 2nd, 4th and 6th order in comparison with exact calculations as an overview (left) and an enlarged section (right).

the leading order coefficient c_0^χ becomes negative for high temperature. This is probably also an effect of the regularization.

Having obtained the coefficients $c_n^\chi(T)$ for the relevant temperature interval, one can calculate the reduced chiral susceptibility using equation (4.14). The behavior of χ_{mm}/T^2 as a function of temperature for various μ/T is shown in figure 4.6. Here we can clearly see that the maximum moves to the left, when μ/T rises. This is the expected effect since the phase boundary has to move to lower temperatures with growing chemical potential.

However it was not expected that the maximum splits up for high μ/T. This behavior will be discussed in more detail in the next figures 4.7 and 4.8, where we compare the values of χ_{mm}/T^2 for expansions to second, fourth and sixth order. In these figures one recognizes several problems concerning the reconstructed chiral susceptibility. Firstly, since the leading order coefficient c_0^χ is negative for high temperatures we have an unphysical zero-crossing and negative susceptibility for high T. Secondly, in the case of $\mu/T = 0.8$ we see that the single local maximum splits up into two local maxima with a (global) minimum in between. Inclusion of higher order terms leads to higher minimum to maximum-amplitude. On the other hand one can clearly recognize that higher order terms shift the

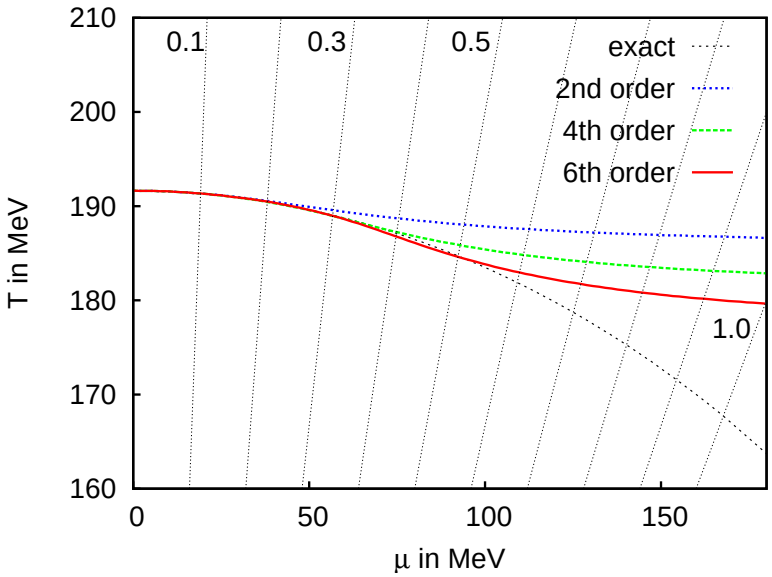

Figure 4.9: Crossover line in the phase diagram calculated using a Taylor series expansion to 2nd, 4th and 6th order in comparison with exact calculation. Lines of constant μ/T are indicated with dotted lines.

maximum to lower temperatures.

As we did before in the exact NJL mean-field case, we will now determine the temperature for which the reduced chiral susceptibility takes its (local) maximum for each μ/T. We have shown that the local maximum splits up starting at a certain value of μ/T. First the left of the two maxima is the higher one (see figure 4.6). In order to have a continuous crossover line we will restrict the search on the leftmost local maximum.

To show the influence of each order, we applied the depicted method on the reduced chiral susceptibility given by eq. (4.14) to 2nd, 4th and 6th order. The crossover lines determined using the reduced chiral susceptibility to different orders are shown in the phase diagram in figure 4.9. We included the result from section 3 for comparison.

The agreement of the crossover line to the exact calculation grows from order to order which is expected from the Taylor series method. As has been visible in figures 4.7 and 4.8, higher order terms push the maximum to lower temperatures, which indeed moves the crossover line closer to the exact one. Using the sixth order result, a good agreement with exact calculation exists for $\mu/T \lesssim 0.55$. This is one seventh of the critical value $(\mu/T)_c = 3.92$.

4.4 Radius of convergence

Coping with a power series we need to have in mind, that the series only converges in a specific range of the argument (here μ/T) which is known as the radius of convergence. For a Taylor series with coefficients c_{2n} the radius of convergence can be obtained using

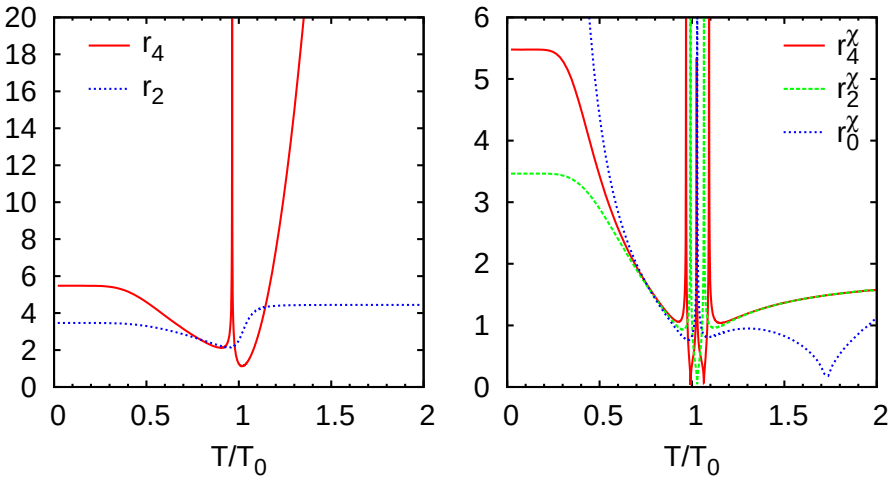

Figure 4.10: Values r_2 and r_4 (left) and r_0^χ, r_2^χ and r_4^χ (right) as defined in eq. (4.17) as functions of T/T_0.

the ratio test:

$$r = \lim_{n\to\infty} r_{2n} = \lim_{n\to\infty} \sqrt{\left|\frac{c_{2n}}{c_{2n+2}}\right|} \tag{4.17}$$

Since we calculated a finite number of coefficients only, we cannot evaluate the limit of n to infinity, but we can examine the evolution of r_{2n} (r_{2n}^χ) for successive coefficients c_{2n} (c_{2n}^χ). The Taylor series expansion was done for a whole range of temperatures, thus the radius of convergence depends on the temperature.

In figure 4.10 we show the values r_2 and r_4 for the coefficients c_{2n} of the reduced thermodynamic potential and the values r_0^χ , r_2^χ and r_4^χ for the expansion coefficients c_{2n}^χ of the reduced chiral susceptibility as functions of temperature. There is no general behavior visible except that most fluctuations appear in the vicinity of T_0. At temperatures where the coefficient in the denominator has a zero-crossing an infinite value occurs. From these graphs one cannot yet extrapolate to $n \to \infty$ so the determination of a radius of convergence for the Taylor series expansions of Ω and χ_{mm}/T^2 is not possible.

5 Conclusion and outlook

We started by introducing a simple NJL Lagrangian for two flavors. With the grand thermodynamic potential and the gap equation we were able to calculate the stable constituent mass and further thermodynamic observables. Chiral symmetry and its restoration could be explained based on dynamic mass generation.

Using the parameter set $G = 2.44\ \Lambda^2$, $m = 5.6$ MeV and $\Lambda = 587.9$ MeV we were able to determine the structure of the phase diagram and found a critical endpoint at $\mu/T = 3.92$ using conventional calculation.

Next, we applied the Taylor series expansion technique to the NJL model. The grand potential was expanded in powers of μ/T at $\mu = 0$. The expansion coefficients as functions of the temperature and their derivatives with respect to the bare quark mass were calculated up to sixth order and compared to results from [ADE$^+$05]. The expansion coefficients perfectly comply with the high temperature (SB) limit when using the special regularization method.

Using the Taylor series expansion we obtained the crossover line via the reduced chiral susceptibility. The crossover line was in good agreement with exact calculation up to $\mu/T = 0.55$, which is only a seventh of the way to the critical endpoint. We were therefore not able to estimate the location of the critical endpoint from the Taylor series expansion.

Besides calculating higher order expansion coefficients which should improve the crossover line beyond $\mu/T = 0.55$, obvious enhancements to the simple NJL model would be to include vector interactions or to break the degeneracy of up and down quarks by assigning them different bare masses and chemical potentials. Furthermore the strange quark could be included as a third quark flavor with a higher bare mass.

The approaches of lattice QCD and the NJL model are very different. Still one could try to match the expansion coefficients obtained by the NJL model with lattice results by changing the NJL parameters. In that way one could estimate the location of the critical endpoint from lattice calculations by determining it in the NJL model using conventional calculation.

A Appendix

A.1 Taylor coefficients

All the following terms have to be evaluated at $\mu = 0$, we will omit any " $\big|_{\mu=0}$" for better reading. Please note, that all stated total derivatives shall act on the arguments $M(T, \mu)$ and μ only.

$$\frac{\partial \Omega_{NJL}}{\partial M} = 0 \quad \text{(gap equation)} \tag{A.1}$$

$$\begin{aligned} d_2(T) = \frac{d\Omega_{NJL}}{d(\mu^2)} &= \frac{\partial \Omega_{NJL}}{\partial(\mu^2)} + \frac{\partial \Omega_{NJL}}{\partial M}\,\frac{\partial M}{\partial(\mu^2)} \\ &= \frac{\partial \Omega_{NJL}}{\partial(\mu^2)} \end{aligned} \tag{A.2}$$

$$2 \cdot d_4(T) = \frac{d^2\Omega_{NJL}}{d(\mu^2)^2} = \frac{\partial^2 \Omega_{NJL}}{\partial(\mu^2)^2} + 2\frac{\partial^2 \Omega_{NJL}}{\partial M \partial(\mu^2)}\,\frac{\partial M}{\partial(\mu^2)} + \frac{\partial^2 \Omega_{NJL}}{\partial M^2}\,\left(\frac{\partial M}{\partial(\mu^2)}\right)^2 \tag{A.3}$$

$$\begin{aligned} 6 \cdot d_6(T) =& \frac{d^3\Omega_{NJL}}{d(\mu^2)^3} = \frac{\partial^3 \Omega_{NJL}}{\partial(\mu^2)^3} + 3\left(\frac{\partial^2 \Omega_{NJL}}{\partial M^2}\,\frac{\partial^2 M}{\partial(\mu^2)^2} + \frac{\partial^3 \Omega_{NJL}}{\partial M \partial(\mu^2)^2}\right)\frac{\partial M}{\partial(\mu^2)} \\ &+ 3\frac{\partial^3 \Omega_{NJL}}{\partial M^2 \partial(\mu^2)}\,\left(\frac{\partial M}{\partial(\mu^2)}\right)^2 + 3\frac{\partial^2 \Omega_{NJL}}{\partial M \partial(\mu^2)}\,\frac{\partial^2 M}{\partial(\mu^2)^2} + \frac{\partial^3 \Omega_{NJL}}{\partial M^3}\left(\frac{\partial M}{\partial(\mu^2)}\right)^3 \end{aligned} \tag{A.4}$$

A.2 Derivatives of $\Omega_{NJL}(T, \mu; M)$

$$C := 2N_c N_f \frac{4\pi}{(2\pi)^3}$$

derivatives with respect to μ^2 only

$$\left.\frac{\partial \Omega_{NJL}}{\partial(\mu^2)}\right|_{\mu=0} = -C \int_0^\infty dk\; k^2\; \frac{1}{2\,T\left[1 + \cosh\left(\frac{E_k}{T}\right)\right]} \tag{A.5}$$

$$\left.\frac{\partial^2 \Omega_{NJL}}{\partial(\mu^2)^2}\right|_{\mu=0} = -C \int_0^\infty dk\; k^2\; \frac{-2 + \cosh\left(\frac{E_k}{T}\right)}{48\,T^3\left[\cosh\left(\frac{E_k}{2T}\right)\right]^4} \tag{A.6}$$

$$\left.\frac{\partial^3 \Omega_{NJL}}{\partial(\mu^2)^3}\right|_{\mu=0} = -C \int_0^\infty dk\; k^2\; \frac{33 - 26\cosh\left(\frac{E_k}{T}\right) + \cosh\left(\frac{2E_k}{T}\right)}{1920\,T^5\left[\cosh\left(\frac{E_k}{2T}\right)\right]^6} \tag{A.7}$$

derivatives with respect to M only

$$\frac{\partial \Omega_{NJL}}{\partial M} = 0 \quad \text{(gap equation)} \tag{A.8}$$

$$\left.\frac{\partial^2 \Omega_{NJL}}{\partial M^2}\right|_{\mu=0} = \frac{1}{2G} - C\left\{\int_0^\Lambda dk \frac{k^4}{E_k^3} - \int_0^\infty dk\, k^2 \left[\frac{k^2}{E_k^3}\frac{2}{e^{\frac{E_k}{T}}+1} - \frac{M^2}{TE_k^2}\frac{2e^{\frac{E_k}{T}}}{\left(e^{\frac{E_k}{T}}+1\right)^2}\right]\right\} \tag{A.9}$$

$$\left.\frac{\partial^3 \Omega_{NJL}}{\partial M^3}\right|_{\mu=0} = \lim_{\Delta\to 0} \frac{\frac{\partial^2 \Omega_{NJL}}{\partial M^2}(M+\Delta) - \frac{\partial^2 \Omega_{NJL}}{\partial M^2}(M-\Delta)}{\Delta} \tag{A.10}$$

mixed derivatives

$$\left.\frac{\partial^2 \Omega_{NJL}}{\partial M \partial(\mu^2)}\right|_{\mu=0} = C\frac{M}{4T^2}\int_0^\infty dk \frac{k^2}{E_k}\frac{\tanh\left(\frac{E_k}{2T}\right)}{\cosh\left(\frac{E_k}{2T}\right)^2} \tag{A.11}$$

$$\left.\frac{\partial^3 \Omega_{NJL}}{\partial M^2 \partial(\mu^2)}\right|_{\mu=0} = -\frac{C}{8T^3}\int_0^\infty dk \frac{k^2}{E_k^3}\frac{M^2 E_k\left[\cosh\left(\frac{E_k}{T}\right)-2\right] - k^2 T\sinh\left(\frac{E_k}{T}\right)}{\cosh\left(\frac{E_k}{2T}\right)^4} \tag{A.12}$$

$$\left.\frac{\partial^3 \Omega_{NJL}}{\partial M \partial(\mu^2)^2}\right|_{\mu=0} = -C\frac{M}{48T^4}\int_0^\infty dk \frac{k^2}{E_k}\frac{\cosh\left(\frac{E_k}{2T}\right)\sinh\left(\frac{E_k}{T}\right) - 2\sinh\left(\frac{E_k}{2T}\right)\left[\cosh\left(\frac{E_k}{T}\right)-2\right]}{\cosh\left(\frac{E_k}{2T}\right)^5} \tag{A.13}$$

A.3 Derivatives of $M(T,\mu)$

$$\left.\frac{\partial M}{\partial(\mu^2)}\right|_{\mu=0} = \lim_{\Delta\to 0}\frac{M(T,\Delta)-M(T,0)}{\Delta} \tag{A.14}$$

$$\left.\frac{\partial^2 M}{\partial(\mu^2)^2}\right|_{\mu=0} = \lim_{\Delta\to 0}\frac{M(T,2\Delta)-2M(T,\Delta)+M(T,0)}{\Delta^2} \tag{A.15}$$

References

[ADE+05] C. R. Allton, M. Döring, S. Ejiri, S.J. Hands, O. Kaczmarek, F. Karsch, E. Laermann, and K. Redlich. Thermodynamics of two flavor QCD to sixth order in quark chemical potential. *Phys. Rev.*, D71:054508, 2005.

[Bub05] M. Buballa. NJL-model analysis of dense quark matter. *Phys. Rep.*, 407:205, 2005.

[Kap89] J. I. Kapusta. *Finite Temperature Field Theory*. Cambridge University Press, 1989.

[Kle92] S. P. Klevansky. The Nambu-Jona-Lasinio model of quantum chromodynamics. *Rev. Mod. Phys.*, 64:649, 1992.

[NJL61a] Y. Nambu and G. Jona-Lasinio. Dynamical model of elementary particles based on an analogy with superconductivity. I. *Phys. Rev.*, 122:345, 1961.

[NJL61b] Y. Nambu and G. Jona-Lasinio. Dynamical model of elementary particles based on an analogy with superconductivity. II. *Phys. Rev.*, 124:246, 1961.

[Phi07] O. Philipsen. Lattice QCD at finite temperature and density, 2007. `arXiv:hep-lat/0708.1293v1`.

[Rip97] G. Ripka. *Quarks Bound by Chiral Fields*. Oxford Science Publications, 1997.

[Sch95] P. Schmüser. *Feynman-Graphen und Eichtheorien für Experimentalphysiker*. Springer, 1995.